18th IMEKO TC10 Conference
"Measurement for Diagnostics, Optimisation and Control to Support Sustainability and Resilience"
Warsaw, Poland, September 26–27, 2022

Failure limit analysis for Li-ion batteries using Ragone plot: a preliminary study

Mirko Marracci[1], G. Caposciutti[1], A. Buffi[1], G. Bandini[1] and B. Tellini[1]

[1]*Department DESTeC, University of Pisa, Largo L. Lazzarino, 56122 Pisa*
email: mirko.marracci@unipi.it

***Abstract* – In this paper, a new possible definition of failure zone for Li-ion batteries is proposed. Based on the general concept that a battery can be considered failed when its performance no longer meets the requirements of the application for which it is designed, a new application-dependent failure zone definition is proposed using the Ragone plot of the cell.**
The results of an experimental campaign to validate the proposal are presented and discussed in the paper.

Keywords – Li-ion batteries, Failure; Ageing.

I. INTRODUCTION

Lithium-ion batteries (LIBs) play a key role in the current energy scenario and are widely used in various application fields ranging from low-power applications, such as portable devices, to electric vehicles [1]. Their stability and efficiency is the basis for their widespread use [2], while performance is steadily increasing in terms of durability, energy and power density [3] and safety of use [4], [5].

The Ragone diagram was originally introduced by D.V. Ragone in [6] to characterize the performance of batteries for vehicular applications. The original idea was to describe the behavior of batteries in terms of two parameters: specific power (related to the speed of the vehicle and its acceleration) and specific energy (related to its range). The two parameters were used to graphically compare (through Ragone plot, precisely) the performance of a range of batteries available at the time (including lead-acid, silver-zinc, nickel-cadmium, organic electrolyte, metal-air and fused-salt).
Over the years, the use of the Ragone diagram has been extended to other types of Energy Storage (ES) devices, such as supercapacitors and fuel cells, and used to allow performance comparisons between the various available technologies. In this perspective, the classic Ragone curves are replaced by areas (zones) in the graph that represent the "typical" performance of the technologies under consideration [7]. An example of such use is shown in Fig. 1

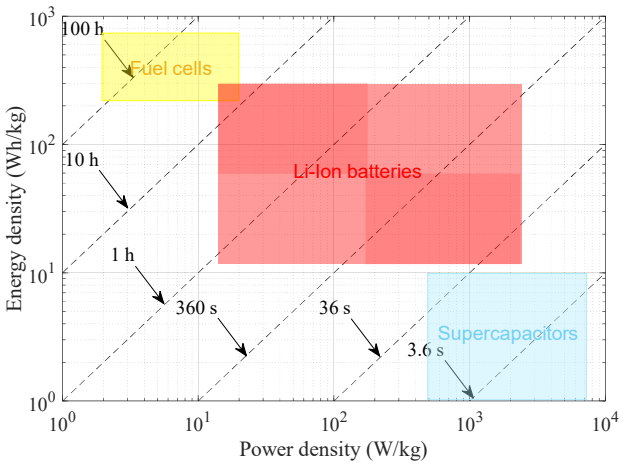

Fig. 1. Operating area of different Energy Storage devices.

It is important to note that the areas depicted in Fig. 1 represent the entire area that can be covered by a given technology, not the performance achievable by a single device of that type. For example, within the red area of Fig. 1 (Li-Ion batteries), the so-called "very high-power" cells will exhibit curves concentrated in the lower right zone of the area attributed to Li-Ion technology (corresponding to high power densities but energy densities lower than the maximum achievable by the technology); on the other hand, high energy cells will exhibit the highest energy densities achievable by the technology but lower power densities and therefore will occupy the upper left part of the red zone in Fig. 1.

II. RAGONE PLOTS AND FAILURE DEFINITION

Let's now consider a possible Ragone diagram of a Li-Ion cell such as the one shown in Fig. 2.

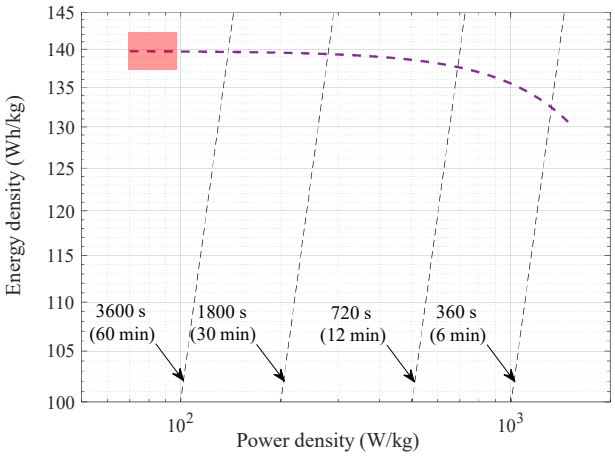

Fig. 2. Ragone plot of a generic Li-ion battery.

The diagram gives a possible power density-energy density curve for a new Li-ion cell. The trend of the curve shows the reduction (limited in the present case) of the energy that can be drawn from the cell as power increases, within the operating parameters specified by the manufacturer.

The aging of the battery, or generally its State of Health (SoH) is normally defined in terms of a reduction in the nominal capacity of the cell and has no immediate correspondence within Ragone diagram. In general, however, it can be said that the cell capacity is stated by the manufacturer for a standard discharge profile, normally defined at low current values (usually 0.2C or 1C, where C is the nominal capacity in Ah of the battery). Although Ragone plot is obtained with constant power discharges while the standard discharge profiles for defining battery capacity are generally at constant current, it is still possible to state that the area investigated for defining battery capacity (nominal or residual) and consequently its SoH is that on the left of the graph (low power discharges), highlighted by a red rectangle in Fig. 2. In particular, the battery capacity Q and its *SoH* can be defined as follows:

$$Q = \int_{t_1}^{t_2} I\,dt \tag{1}$$

$$SoH = \frac{Q}{Q_{nom}} \tag{2}$$

In Eq.1, I is the circulating current, t is the time, and t_1 and t_2 are the start and the end, respectively, of a charge or discharge phase. In Eq.2, Q_{nom} is the nominal capacity provided by the manufacturer.

The definition of failure (or end-of-life) of a battery is generally referred to by industry standards as a reduction in its available capacity i.e. SoH by 15%, 20% or 30%, depending on the specific application. Considering a standard discharge profile at relatively low current (and therefore low power) for defining the residual capacity of the battery and consequently the possible failure of the cell, means defining a failure zone limited to the left side of the Ragone diagram, as shown in the gray zone of Fig. 3 (in the present case, a 15% reduction in the energy density is considered as example).

The trend in Fig. 2 should highlight how a simple threshold indication (e.g. a 15% decrease in the capacity value at low power levels) cannot be well representative of a failure condition and does not take into account the application field in which the battery operates.
In this case, the use of Ragone diagram could help to define new failure conditions, dependent on the application and on the use for which the cell was designed and chosen.

For example, if the battery under consideration is of the "high-power" type and was designed to operate at high currents (and consequently high power densities), the failure area defined in blue in Fig. 3 might be more appropriate.

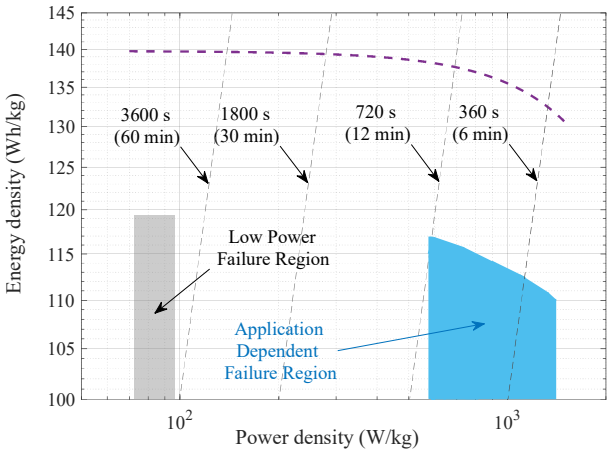

Fig. 3. Possible failure regions of Li-ion battery. Gray area: 15% reduction of the available energy at low power; Blue area: 15% reduction of the available energy for power densities between 580 W/kg and 1400 W/kg (application-dependent).

To analyze the impact of the proposed new definition of application-dependent failure regions, an experimental set-up and measurement campaign were performed to analyze the aging and possible failure of commercial lithium batteries of the 18650 type. In particular, we measured the specific Ragone plot of a battery in two different State of Health conditions, thus assessing the performance decay in light of the aforementioned discussion.

III. DEVICES UNDER TEST

The devices under test (DUTs) adopted in the present study

are Samsung INR 18650-20S cylindrical commercial Lithium cells, shown in Fig. 4. The main DUT specifications declared by the manufacturer are reported in Tab.1.

Fig. 4. Adopted Devices Under Test

Table 1. Specification of INR 18650-20S

Item	Specification
Nominal Capacity	2000 mAh (0.2C, 2.5V discharge)
Minimum Capacity	1950 mAh (0.2C, 2.5V discharge)
Nominal Voltage	3.60 V
Charging Voltage	4.20 V
Standard discharge cycle	0.2C (400 mA), 2.5V cut-off @ RT
Standard charge cycle	CCCV[a], 1.0 A, 4.20V, 100mA or 160 min cut-off
Discharge Cut-off Voltage	2.5 V
Rapid discharge cycle	I = 10 A
Rapid charge cycle	CCCV, 4 A, 4.20V, 100mA or 60 min cut-off
Operating temperature	0 to 50 °C (charge) and -20 to 80 °C (discharge)
Cell Weight	48.0 g (max)

[a.] Constant Current-Constant voltage cycle

As shown in Table 1, the declared nominal capacity is 2.0 Ah for a nominal voltage of 3.6 V for a maximum cell weight of 48.0 g.
The cell capacity (both charging and discharging) is strongly dependent on temperature. Specifically, the stated discharge capacities are guaranteed for a cell operating temperature of 25 °C while they drop at both lower (80% of C_{max} @ 0 °C) and higher temperatures (80% of C_{max} @ 40 °C). Therefore, tests to characterize cell performance will be performed inside a temperature-controlled climate chamber, as further described in the following section.

IV. EXPERIMENTAL SETUP AND PROCEDURE

A Toellner 8871 power supply and a EA-EL 9080-510 electronic load are used to charge-discharge the cells. Both devices are controlled via GPIB through a software developed in the Labview© environment that also allows control of the entire experiment. A shunt resistor in series with the battery is used to measure the current circulating through the device under test (DUT). The latter is placed inside a Genviro 060LC climate chamber to control the external temperature of the cell. The climate chamber can control the temperature with a declared total accuracy of 0.3 °C and spatial accuracy of 1.5 °C, in the range from -70 °C to +180 °C. Two Pt100 1/10 DIN thermal resistance detectors (RTD) are used to monitor the temperature in proximity and nearby the battery for thermal monitoring. A NI cDAQ 9174 chassis equipped with a NI-9219 100 S/s/ch, 4-Channel Analog Input Module is adopted to acquire the temperature and voltage signal from the shunt resistor and from the DUT, thus measuring the battery temperature, the circulating current and the battery voltage over time. A sketch of the system and a picture of the adopted instruments are shown in Fig. 5.

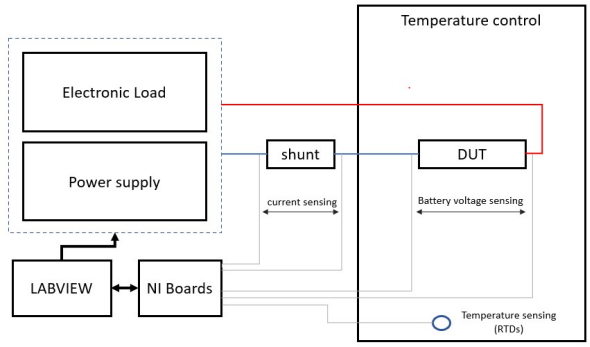

(a)

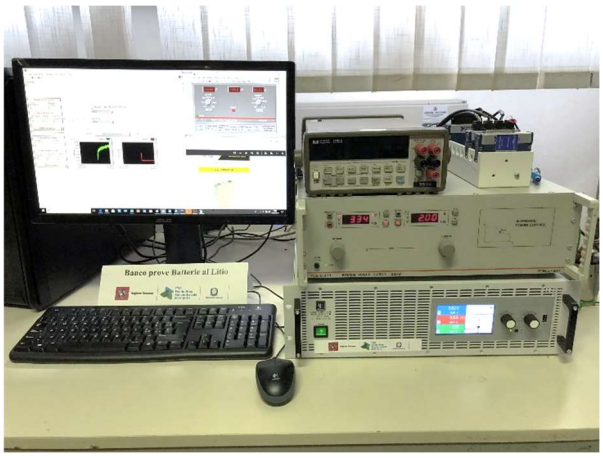

(b)

Fig. 5. Scheme of the measurement system (a), picture of the adopted instruments (b).

In this study, the DUT is firstly trained with 4 CCCV cycles, then the cell is aged by using the "rapid" conditions

reported in Tab.1. However, the discharge current was increased up to 20 A (within the limit of 30 A) and the temperature is set to 45 °C, both in order to accelerate the aging process. While measuring the Ragone plot values, the aging was suspended and the cell is charged within nominal conditions, and discharged at constant power within the maximum current and temperature allowed by the manufacturer specification. Therefore, we measured a first Ragone plot after 10 cycles, and a second one at 205 cycles for comparison purposes. The Energy E and the power P are calculated according to Eq.3 and Eq.4 as follows:

$$P = I\,V \tag{3}$$

$$E = \int_{t_1}^{t_2} I\,V\,dt \tag{4}$$

In Eq. 3, V is the battery voltage, while in Eq.4 the t_1 and t_2 are the start and the end, respectively, of a constant power discharge phase. We highlight that the constant power discharge is operated until the threshold voltage is reached and within the current and temperature limit imposed by the manufacturer.

V. RESULTS AND DISCUSSIONS

As example, the ageing cycles, and the Ragone plot test cycles are reported in Fig.

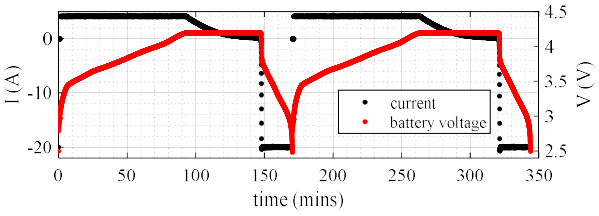

(a)

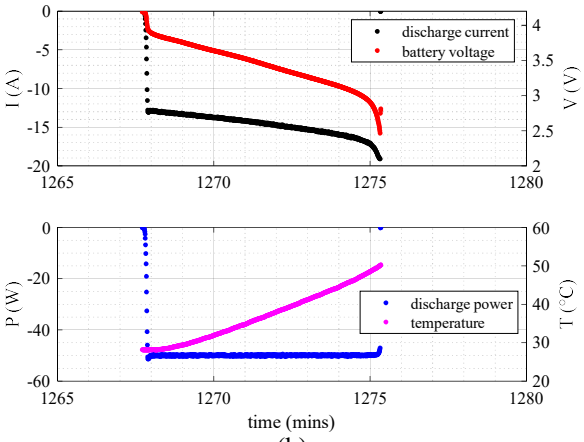

(b)

Fig. 6. Example of ageing cycles (a) and discharge cycle for Ragone plot evaluation at 50 W (b).

In particular, Fig.6 shows that the critical current zone is the final part of the constant power cycle, where the low battery voltage might eventually require large current to maintain the desired discharge power. Moreover, the temperature can result in a limiting factor for the present analysis, being increasing with an approximately constant rate along the whole discharge. On the other hand, after the discharge phase a settle time is used to cool down the cell within the required charge thermal range.

The obtained aging, in terms of residual capacity and *SoH*, is presented in Fig. 7.

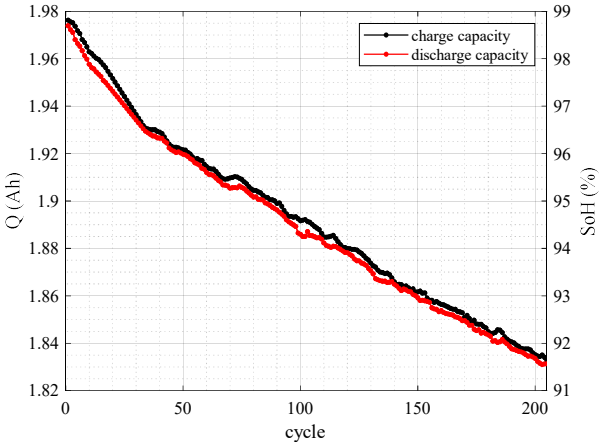

Fig. 7. Charge (black) and discharge (red) capacity for a DUT during a power cycling ageing process in "rapid" conditions.

According to the results presented in Fig.7, we evaluated the Ragone plot values after 10 cycles approximately at 98% *SoH*, and at 205 cycles approximately at 91.5% *SoH*. Therefore, the further results are compared by considering an overall decay of 6.5% *SoH*.

The experimentally obtained Ragone plot for the DUT is shown in Fig. 8.

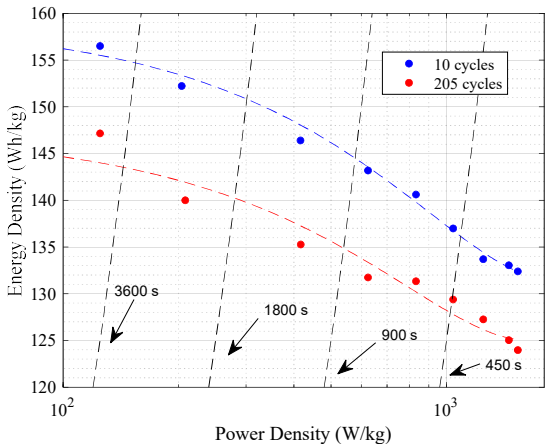

(a)

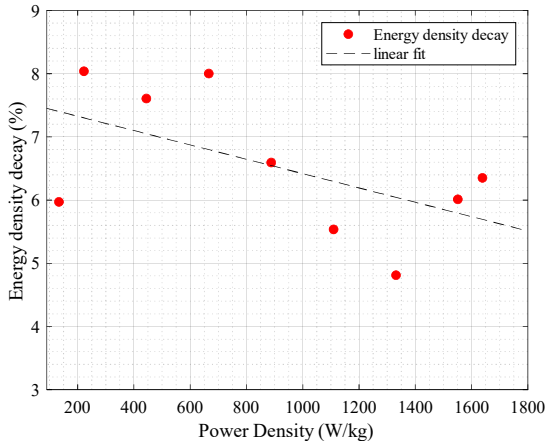

(b)

Fig. 8. Ragone plot experimentally obtained for the new DUT (a) and energy density decay among the Ragone plot values at 10 and 205 cycles, respectively (b)

Fig. 8 shows that, even at this early stage of ageing, the energy reduction is not constant throughout the Ragone Plot. In the present case in particular, we notice an increase in energy reduction (with values close to 8%) in the range of power densities between 200 and 800 W/kg while this reduction tends to be lower at higher power densities (as highlighted by the linear fitting line in Fig. 8b).

The result obtained, although preliminary, suggests a potentially different effect of ageing within the Ragone Plot and confirms the validity of the proposed approach to use an area within the Ragone Plot that is dependent on the application and use for which the battery was designed and chosen to define a potential failure condition.
In addition, different types of failure conditions (e.g., as a result of calendar aging, cycling aging, overcurrents, overvoltages, etc.) can in principle lead to different impacts on the Ragone plot of the cell, confirming the validity of the proposal of a new "application dependent" failure region definition.

VI. CONCLUSIONS AND OUTLOOK

In this paper, a new possible definition of failure zone for Li-ion batteries was proposed and discussed. The end-of-life criterion followed the general definition that a battery fails when its performance no longer meets the requirements of the application.
This led to the proposal of a possible new definition of failure region in the Ragone plot of the cell, as a function of the specific application for which the battery is designed and chosen.
We analysed the performance of a 2 Ah Lithium battery by evaluating its Energy density as a function of its power density at two different ageing states.
The results showed a potentially different impact of ageing on the cell's Ragone plot (and consequently for various discharge powers) and confirm the potential usefulness of a new definition of fault region within the Ragone plot itself, which is application-dependent.

REFERENCES

[1] **C. Iclodean, B. Varga, N. Burnete, D. Cimerdean, and B. Jurchis**, "Comparison of different battery types for electric vehicles," IOP Conference Series: Materials Science and Engineering, vol. 252, p. 012058, oct 2017.

[2] **P. K. Nayak, L. Yang, W. Brehm, and P. Adelhelm,** "From lithium-ion to sodium-ion batteries: Advantages, challenges, and surprises," Angewandte Chemie International Edition, vol. 57, no. 1, pp. 102–120, 2018.

[3] **X. Lv, W. Wei, B. Huang, and Y. Dai**, "Achieving high energy density for lithium-ion battery anodes by si/c nanostructure design," J. Mater. Chem. A, vol. 7, pp. 2165–2171, 2019.

[4] **S. Ciorba, M. Marracci, C. Antonetti, M. Martinelli, G. Caposciutti, B. Tellini, and A. M. Raspolli Galletti,** "Experimental analysis of overcharged li-polymer batteries," Case Studies in Chemical and Environmental Engineering, vol. 2, p. 100012, 2020.

[5] **G. Xu, L. Huang, C. Lu, X. Zhou, and G. Cui,** "Revealing the multilevel thermal safety of lithium batteries," Energy Storage Materials, vol. 31, pp. 72 – 86, 2020.

[6] **Ragone, David V.**: Review of battery systems for electrically powered vehicles. No. 680453. *SAE Technical Paper*, 1968

[7] **Thomas Christen, Martin W. Carlen**, Theory of Ragone plots, *Journal of Power Sources*, Volume 91, Issue 2, 2000, Pages 210-216,

[8] **Yuan Ci Zhang, Olivier Briat, Loïc Boulon, Jean-Yves Deletage, Cyril Martin, Fabio Coccetti, Jean-Michel Vinassa**: Non-isothermal Ragone plots of Li-ion cells from datasheet and galvanostatic discharge tests, *Applied Energy*, Volume 247, 2019, Pages 703-715,